An Accurate Method for Measuring the Sheet Impedance of Thin Conductive Films at Microwave and Millimeter-Wave Frequencies

Xu-Chen Wang, Ana Díaz-Rubio, and Sergei A. Tretyakov, *Fellow, IEEE*

***Abstract*— A simple and accurate method to measure the complex sheet impedance of thin conductive films on dielectric substrates is reported. This method allows for accurate extraction of the sheet impedance without characterizing the substrate (thickness and permittivity) beforehand, within a wide range of frequencies and sheet complex impedances. In this method, the sample is placed between two rectangular waveguide flanges, creating a discontinuity. The discontinuity is modeled by an equivalent Π-circuit, and the sheet impedance is found from measured circuit parameters of the sample and bare substrate. We propose two retrieval approaches using different circuit parameters, examine their extraction accuracy with various substrate thicknesses and sheet impedances, and determine the most reliable extraction method. Uncertainty analysis under random perturbations of measured scattering parameters is also performed to investigate the robustness of the technique. Experimental studies are carried out to demonstrate the validity of the proposed approach for the impedance measurements of thin conductive ink films supported by both thin or thick (up to 0.28 times the wavelength in the dielectric) substrates.**

***Index Terms*— Conductive ink, measurement, millimeter waves, rectangular waveguide, sheet impedance.**

I. Introduction

SHEET impedance is an important electrical parameter of thin conductive material layers, which relates the electric surface current density and the tangential electric field on the sheet plane. Measurements of microwave and millimeter-wave sheet impedance of conductive films are necessary for qualifying a material in practical application. Many efforts have been made in the development of measurement methods for sheet impedance of thin films. For measuring highly conductive films, most methods concentrate on using resonant cavities [1]–[5]. While such techniques can potentially provide high sensitivity and accuracy due to high quality factors of resonators, they are necessarily limited to a few discrete frequency points. To investigate the frequency dependence of sheet impedance, transmission/reflection methods have been employed, as reported in [6]–[8]. Coplanar waveguide-based techniques can measure the impedance within a large frequency range (from 0 to 120 GHz) [6], but with some drawbacks, such as the necessity of patterning the samples and the influence of the contact resistance between the thin films and metal strips. The method in [9] allows extraction of the sheet impedance of a thin film on a substrate by evaluating the power transmitted through the sample, but it can determine only the sheet resistivity. Free-space measurements can be used in a wide frequency range from microwave even to terahertz band [6], [7]. In this method, both thickness and permittivity of the substrate should be known in advance. Moreover, the size of the sample has to be large compared with the wavelength. These difficulties can be overcome if the reflection/transmission measurements are made in rectangular waveguides, since it is possible to achieve strict confinement of wave propagation [10], [11].

For sheet impedance measurements in rectangular waveguide setups, the sample positioning is a crucial issue. If one cuts a sample to the size of the waveguide cross section and inserts it into a waveguide, it is practically impossible to ensure accurate orthogonal placement of the sample and good ohmic contact between the conductive layer and the walls of the waveguide. There are always small gaps, whose parasitic capacitance cannot be ignored [11]. To ensure contact of the thin layer with the waveguide walls, printed areas are placed between two flanges of a waveguide connection [10]. However, in this case, the two metal flanges are not galvanically connected, since there is a dielectric substrate of the sample between the two metal waveguides (see Fig. 1). In this case, the junction reactances and energy leakage along the parallel flange plates need to be carefully considered for avoiding severe errors in the extracted values of the sheet impedance. In a word, the drawbacks of the existing methods hinder the development of novel devices based on thin materials such as graphene, silver nanowire composites, and conductive polyaniline films in microwave and millimeter-wave bands.

In particular, accurate measurement of sheet impedance is urgently needed in the fast-developing ink printing technologies. These emerging technologies are believed to be promising strategies for the fabrication of low-cost, high efficiency, and large-area electronics and photonics [12]–[14]. Different printing methods such as screen printing, inkjet printing, offset, and reverse offset (RO) printing [15]–[18] were reported in the past years. In these methods, the usual thickness of deposited ink films is of the order of 100 nm, which is much less than the skin depth at millimeter-wave frequencies. Therefore, the ink film can be treated as a negligible thickness layer characterized by its sheet impedance. The electrical

Manuscript received December 22, 2016; revised April 27, 2017; accepted May 22, 2017. Date of publication August 7, 2017; date of current version December 12, 2017. This work was supported in part by the Academy of Finland through the LATERA project. *(Corresponding author: Xu-Chen Wang.)*

The authors are with the Department of Electronics and Nanoengineering, Aalto University, 13000 Aalto, Finland (e-mail: xuchen.wang@aalto.fi).

Color versions of one or more of the figures in this paper are available online at http://ieeexplore.ieee.org.

Digital Object Identifier 10.1109/TMTT.2017.2714662

0018-9480 © 2017 IEEE. Translations and content mining are permitted for academic research only. Personal use is also permitted, but republication/redistribution requires IEEE permission. See http://www.ieee.org/publications_standards/publications/rights/index.html for more information.

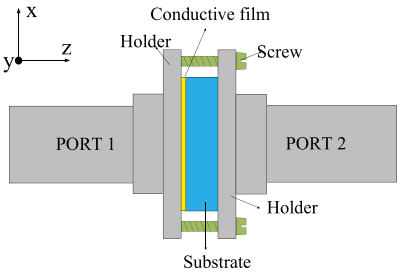

Fig. 1. Schematic of the experimental setup.

properties of ink films depend on the printing technology and sintering treatment (e.g., thermal, laser, and flash lamp annealing), varying several orders of magnitude [19]. For this reason, it is essential to measure the sheet impedance of printed ink layers at the frequency of interest.

In this paper, in order to measure the sheet impedance of thin conductive layers and, in particular, conductive ink films, we propose an accurate impedance extraction method employing a rectangular waveguide. In this method, based on the transmission-line model of the waveguide setup, we can effectively remove the impact of the discontinuity between the two sections of the waveguide with the measured sample between them. The method is shown to be accurate for the retrieval of sheet impedance in a wide range of frequencies and impedance levels without prior characterization of the substrate (its permittivity and thickness).

This paper is organized as follows. In Section II, we introduce alternative extraction methods applying the transmission-line theory. In Section III, we numerically evaluate the accuracy of these methods, the effects of the substrate thickness, and the robustness under assumed random uncertainty of measurements. In Section IV, we present an experiment validation of this measurement technique.

II. Measurement Setup and Retrieval Methods

In the proposed measurement method, a rectangular waveguide with the cross-section dimensions $a \times b$ operating in its fundamental TE_{10} mode is employed for wave confinement. The thin film, which is deposited on one side of a dielectric substrate, is fixed between two waveguide flanges, as shown in Fig. 1. The measurement comprises two steps: 1) characterization of the gap between the two waveguide sections after the insertion of a naked substrate sample (no deposition) and 2) characterization of the conductive film deposited on the substrate. Combining the results obtained in both steps allows us to accurately extract the sheet impedance of thin film, eliminating the influence of the waveguide gap and the substrate.

A. Characterization of the Waveguide Gap

The measurement cell consists of four parts (see Fig. 1): the dielectric substrate, two metal flanges, and the metallic screws. The thin conducting film under test is positioned in a gap between the dielectric substrate and one of the waveguide flanges. Theoretically, the complex environment in the gap can be modeled by an equivalent Π-circuit. In the most general case, the circuit is defined by three independent components (called gap parameters): a series impedance, Z_{g3}, and two parallel admittances, Y_{g1} and Y_{g2}. Since the waveguide gap with only naked substrate is a symmetric system, in this case, the two parallel admittances are equal ($Y_{\mathrm{g1}} = Y_{\mathrm{g2}} = Y_{\mathrm{gp}}$). This Π-circuit can be described in terms of its *ABCD* matrix as follows:

$$\begin{bmatrix} A & B \\ C & D \end{bmatrix} = \begin{bmatrix} 1 & 0 \\ Y_{\mathrm{gp}} & 1 \end{bmatrix} \begin{bmatrix} 1 & Z_{\mathrm{g3}} \\ 0 & 1 \end{bmatrix} \begin{bmatrix} 1 & 0 \\ Y_{\mathrm{gp}} & 1 \end{bmatrix} = \begin{bmatrix} 1 + Z_{\mathrm{g3}} Y_{\mathrm{gp}} & Z_{\mathrm{g3}} \\ Z_{\mathrm{g3}} Y_{\mathrm{gp}}^2 + 2Y_{\mathrm{gp}} & 1 + Z_{\mathrm{g3}} Y_{\mathrm{gp}} \end{bmatrix}. \quad (1)$$

Each element in (1) can be expressed in terms of the *S*-parameters of the setup [20]. We can now equate respective elements of the *ABCD* matrix expressed in terms of the equivalent circuit parameters (1) and in terms of the measured *S*-parameters. Since the matrix element $B = Z_{\mathrm{g3}}$, we can calculate Z_{g3} from the measured *S*-parameters directly

$$Z_{\mathrm{g3}} = Z_0 \frac{(1 + S_{11})^2 - S_{21}^2}{2S_{21}}. \quad (2)$$

Here $Z_0 = \omega\mu_0/(\omega^2\mu_0\epsilon_0 - (\pi/a)^2)^{1/2}$ is the characteristic impedance of the TE_{10} mode in the waveguides. In order to determine Y_{gp}, we can either equate $A(= D)$ or C to their expressions in terms of the *S*-parameters. From simulations and experiments, we find that the value of C is much less sensitive to setup imperfections than the values of A and D. Moreover, due to inevitable small asymmetries in the setup, A is not exactly equal to D. For these reasons, we find Y_{gp} equating the matrix element C to its expression in terms of the *S*-parameters

$$Z_{\mathrm{g3}} Y_{\mathrm{gp}}^2 + 2Y_{\mathrm{gp}} = \frac{(1 - S_{11})^2 - S_{21}^2}{2S_{21}Z_0}. \quad (3)$$

In this way, we minimize the effects of small parasitic fluctuations of the measured Z_{g3} on the extracted results. Note that (3) has two solutions for Y_{gp}, and the solution with a negative conductance should be dismissed since the gap is passive.

B. Extraction of Sheet Impedance

The second step for determining the sheet impedance is the characterization of the conductive membrane deposited on one side of the substrate. Since the waveguide cross section is entirely covered with the impedance sheet, the transmission-line model of the measurement cell has the structure depicted in Fig. 2, where the thin layer is modeled by a parallel admittance Y_{s}. Following the same approach as in the previous step, the *ABCD* matrix of the gap with the thin layer under test is written as:

$$\begin{bmatrix} A' & B' \\ C' & D' \end{bmatrix} = \begin{bmatrix} 1 & 0 \\ Y_{\mathrm{s}} & 1 \end{bmatrix} \begin{bmatrix} 1 & 0 \\ Y'_{\mathrm{g1}} & 1 \end{bmatrix} \begin{bmatrix} 1 & Z'_{\mathrm{g3}} \\ 0 & 1 \end{bmatrix} \begin{bmatrix} 1 & 0 \\ Y'_{\mathrm{g2}} & 1 \end{bmatrix} = \begin{bmatrix} 1 + Z'_{\mathrm{g3}} Y'_{\mathrm{g2}} & Z'_{\mathrm{g3}} \\ (Y_{\mathrm{s}} + Y'_{\mathrm{g1}})(Z'_{\mathrm{g3}} Y'_{\mathrm{g2}} + 1) + Y'_{\mathrm{g2}} & Z'_{\mathrm{g3}}(Y_{\mathrm{s}} + Y'_{\mathrm{g1}}) + 1 \end{bmatrix}. \quad (4)$$

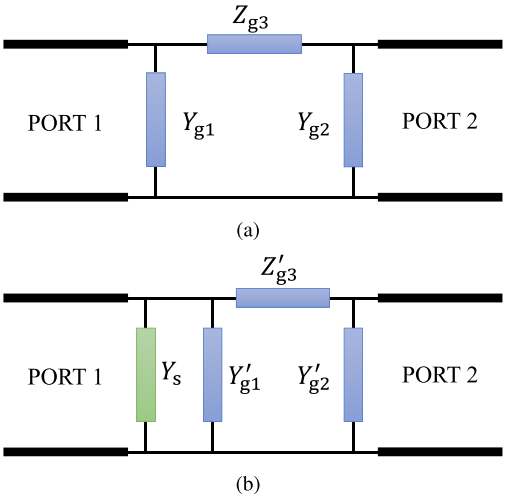

Fig. 2. Equivalent transmission-line model of the setup for two scenarios. (a) Bare substrate ($Y_{g1} = Y_{g2} = Y_{gp}$). (b) Substrate with impedance sheet.

For solving Y_s from the measured S-parameters, some important aspects must been taken into consideration for ensuring the accuracy of the method. In the proposed setup, as it was demonstrated in [10], the extracted impedance is quite sensitive to the errors in measured reflection coefficients if the impedance sheet is highly reflective and the reflection coefficient is close to unity. Therefore, it is desirable to avoid the use of the reflection coefficients in extraction procedures. The transmission coefficient can be expressed as a function of the A', B', C', and D' parameters of the cell in the presence of the thin film as follows [20]:

$$S'_{21} = \frac{2}{A' + B'/Z_0 + C'Z_0 + D'}. \tag{5}$$

Equation (5) has four unknowns, Y'_{g1}, Y'_{g2}, Z'_{g3}, and Y_s. If we assume that the parameters of the gap structure with a bare dielectric sheet do not significantly change due to the film presence, that is, $Y_{gp} = Y'_{g1} = Y'_{g2}$ and $Z_{g3} = Z'_{g3}$, we can easily solve Y_s from (5) knowing the measured S'_{21}. The sheet impedance $Z_s = 1/Y_s$ can be written as

$$Z_s = \frac{S'_{21}(Z_0 Z_{g3} Y_{gp} + Z_{g3} + Z_0)}{2 - S'_{21}\left[Z_{g3}Y_{gp}(Z_0 Y_{gp} + 2) + \frac{Z_{g3}}{Z_0} + 2Y_{gp}Z_0 + 2\right]} \tag{6}$$

where Z_{g3} and Y_{gp} are obtained from the characterization of the waveguide gap. In the following, we denote this approach that uses only the transmission coefficient S'_{21} by Approach I. In this extraction scenario, we completely overcome the problem of the use of the reflection coefficient, which can be rather close to unity in the absolute value, but we have to assume that the equivalent parameters of the measuring cell do not change due to the presence of the thin layer. This assumption, however, is an approximation, which can degrade the impedance extraction accuracy.

We propose to improve the extraction accuracy by also measuring the reflection coefficient, but from the back side of the measurement cell. Even if the impedance sheet is highly conductive, $|S'_{22}|$ is not so large as $|S'_{11}|$. Comparing with reflections from port 1 (the ink surface), considerably more energy leaks away into free space via the gap or is lost in the substrate. This approach allows us to use the measured S'_{22} to relax the strong assumptions of Approach I, since we can remove the assumptions that the cell parameters do not change when we introduce the impedance sheet and we can determine how either Z_{g3} or Y_{gp} changes. Numerical and experimental studies show that Z_{g3} is more susceptible to the presence of conductive sheets and to small structural variations of the setup (see Sections III and IV). Therefore, it is reasonable to remove the assumption that $Z'_{g3} = Z_{g3}$ using the measured S'_{22}. In this approach, we take advantage of the gap leakage (usually considered as a severe negative factor, which limits the accuracy of the measurements and the range of measurable parameters [10]) to improve the measurement accuracy.

Obviously, S'_{22} is also a function of A', B', C', and D', and it can be expressed as

$$S'_{22} = \frac{-A' + B'/Z_0 - C'Z_0 + D'}{A' + B'/Z_0 + C'Z_0 + D'}. \tag{7}$$

Combining (5) and (7), we get two equations

$$\frac{1 + S'_{22}}{S'_{21}} = \frac{B' + D'Z_0}{Z_0} = \frac{Z'_{g3}}{Z_0} + Z'_{g3}\left(Y_s + Y'_{g1}\right) + 1 \tag{8}$$

$$\frac{1 - S'_{22}}{S'_{21}} = A' + C'Z_0 = \left(Y_s + Y'_{g1}\right)Z_0\left(Z'_{g3}Y'_{g2} + 1\right) + Y'_{g2}Z_0 + Z'_{g3}Y'_{g2} + 1. \tag{9}$$

Assuming that Y'_{g1} and Y'_{g2} are equal to Y_{gp} obtained in the characterization of the bare substrate in the gap, the sheet impedance of the conductive layer $Z_s = 1/Y_s$ can be obtained from the solution of equation set (8) and (9)

$$Z_s = \frac{S'_{21}Z_0}{1 - S'_{22} - S'_{21} - Z_0 Y_{gp}\left(1 + S'_{22} + S'_{21}\right)}. \tag{10}$$

We denote this approach as Approach II.

In this paper, Approaches I and II are also compared with the simple extraction method used in [10], where the effects of the gap are not considered. In [10], the two separate waveguide sections are viewed as a continuous waveguide even with insertion of the sample. The extraction formula for the sheet impedance follows from the assumption that the thin layer is a series insertion in a TE_{10}-mode waveguide, and it reads:

$$Z_s = \frac{-S'_{21}Z_0 Z_d\left(Z_0\cos(k_z d) + jZ_d\sin(k_z d)\right)}{2Z_0 Z_d\left(S'_{21}\cos(k_z d) - 1\right) + j\left(Z_0^2 + Z_d^2\right)S'_{21}\sin(k_z d)} \tag{11}$$

where $k_z = (\omega^2\mu_0\epsilon_r - (\pi/a)^2)^{1/2}$ is the propagation constant of the TE_{10} mode in the substrate-filled waveguide, $Z_d = \omega\mu_0/k_z$ is the characteristic impedance of this waveguide section, and d and ϵ_r denote the thickness and the relative dielectric permittivity of the substrate, respectively. The physical parameters of the dielectric substrate (d and ϵ_r) should be characterized before using (11).

III. Numerical Analysis

There are two main sources of retrieval errors: the approximate nature of the extraction formulas and measurement errors in measured S-parameters. In this section, we first investigate the theoretical accuracy of the two extraction approaches proposed in this paper, using numerical simulations (Ansoft HFSS). Here, we assume that the S-parameters are known exactly. The uncertainties due to experimental errors in measured S-parameters are studied next.

A rectangular waveguide with the dimensions 2.54 mm × 1.27 mm is modeled, including two metallic holders for fixing the samples (see Fig. 1). The dimensions of the metallic holders are 22 mm × 20 mm. The range of frequencies under study is from 75 to 110 GHz, ensuring that only TE_{10} mode is propagating in the waveguides. In this analysis, a flexible polyimide substrate with the thickness of $d = 125\ \mu$m ($\approx 0.07\lambda_d$) is used as a dielectric substrate (λ_d is the wavelength of TEM waves in the dielectric layer at 95 GHz). The complex relative permittivity of the substrate in the frequency band from 75 to 110 GHz is assumed to be $3.2(1-j0.045)$. We arbitrarily select a dielectric substrate size (5 mm × 5 mm), which can fully cover the rectangular waveguide openings of the holders (2.54 mm × 1.27 mm). The impedance layer is placed on one side of the substrate (covering all the substrate area).

A. Extraction Accuracy Versus Frequency

We start with the extraction of the sheet impedance defined as $Z_s = 100 + j50\ \Omega/\text{sq}$ in the frequency range from 75 to 110 GHz. Fig. 3(a) shows a comparison of the results given by the extraction formulas proposed in this paper (Approaches I and II) and in [10], where a continuous waveguide is assumed. It can be observed from Fig. 3(a) that the method in [10] gives significant errors (about 20%) and the extracted curve is not flat as a function of the frequency.

As we can see in Fig. 4, the error considerably increases with the dielectric substrate thickness. This is because some energy leaks out from the gap when passing from port 1 to port 2, and the measured transmitted power is always smaller than the power transmitted through the impedance sheet. As a result, the extracted impedance using (11) appears lower than its exact value.

In a striking contrast with the method in [10], we can see from Fig. 3(a) that Approaches I and II give much smaller errors in the extraction of both resistive and reactive parts of the sheet impedance. Approach II, which does not assume that $Z'_{g3} = Z_{g3}$, gives more accurate results than Approach I. Within the considered frequency window, the extracted values from Approach II keep constant while there are some perturbations in the results given by Approach I. The perturbations are caused by the differences between Z'_{g3} and Z_{g3}, as seen from Fig. 3(b). The disagreement of the series impedance Z_{g3} between the two cases is due to slight changes of the field distribution in the presence of the impedance sheet.

B. Extraction Accuracy Versus Gap Thickness

The impact of the gap thickness on the retrieval accuracy of the two approaches is seen in Fig. 4. For a given value of the sheet impedance $Z_s = 100\ \Omega/\text{sq}$ at a single frequency point $f = 95$ GHz, we have extracted the impedance values from the S-parameters for different thicknesses of the setup gap (from $0.05\lambda_d$ to $0.8\lambda_d$).

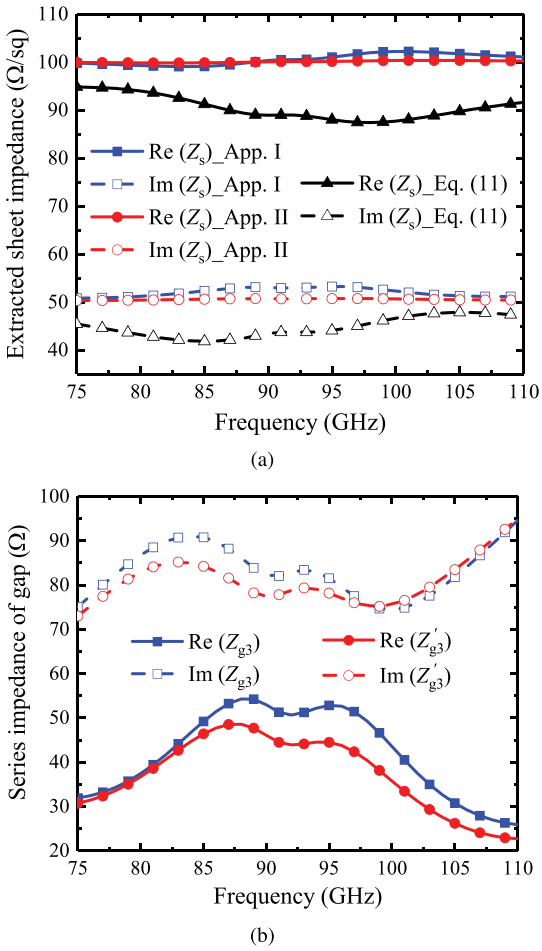

Fig. 3. (a) Extracted sheet impedance using Approaches I and II, and also (11), assuming the exact value is $Z_s = 100 + j50\ \Omega/\text{sq}$. (b) Extracted values of Z'_{g3} and Z_{g3}.

It is expected that close to the Fabry–Perot resonant thickness $d = \lambda_d/2$, the methods based on measurements of the transmission coefficient fail, and we indeed observe parasitic peaks in the extracted values. On the other hand, for $d < \lambda_d/2$, both of the proposed approaches exhibit small errors. Obviously, Approach II performs better than Approach I and its extracted curves are almost flat with the increase of the thickness.

The validity of the proposed methods for $d < \lambda_d/2$ is ensured by nearly unaltered field pattern inside the measuring cell behind the impedance sheet. Fig. 5(a) displays the calculated field pattern in the gap for the thickness $d = 0.17\lambda_d$. For the case of a naked substrate [Fig. 5(a, left)], the electric field is still TE_{10} mode in the region projected from the waveguide cavity [denoted by the "cavity region" in Fig. 5(a)], while between the metal holders, the field is perpendicular to the surface of the holders and propagates along the gap in form of a TEM wave. Importantly, the field pattern remains nearly the same in the presence of the impedance sheet [Fig. 5(a, right)],

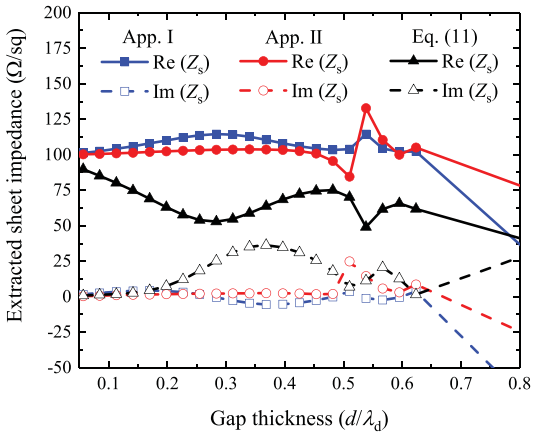

Fig. 4. Estimated sheet impedance at $f = 95$ GHz in terms of the thickness of the gap using different methods. The assumed sheet impedance is $Z_s = 100\ \Omega$/sq.

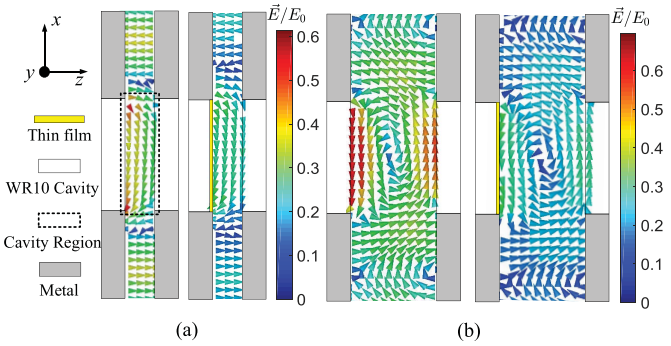

Fig. 5. Effect of the substrate thickness variation on the the field distribution in the gap. (a) Electric field distribution in the gap ($d = 0.17\lambda_d$). Left: the naked substrate. Right: the substrate with the impedance sheet. (b) Electric field distribution in the gap ($d = 0.56\lambda_d$). The assumed sheet impedance is $Z_s = 100\ \Omega$/sq in both (a) and (b).

which means that the gap parameters in the two cases (the substrate with and without the impedance sheet) are almost identical. This property supports the assumption made in the extraction procedures of Approaches I and II.

In contrast to conventional extraction methods based on the measured transmission coefficient (such as the Nicolson–Ross–Weir method), when the thickness of the gap is larger than $\lambda_d/2$ but not close to higher order Fabry–Perot values, the extraction accuracy remains poor. This is caused by higher order modes (in particular, TM_1 mode), which propagate in the parallel plate waveguide formed by the holders, as is seen in Fig. 5(b). In this situation, the gap parameters are affected not only by the TEM mode but also by the TM_1 mode. Since the sheets with different impedances excite the TM_1 mode with unequal magnitudes and different phases, this effect greatly increases the uncertainties of the gap parameters when different impedance sheets are measured. Therefore, the proposed extraction methods should be used for substrates with $d < \lambda_d/2$, where the accuracy is rather good and stable.

C. Extraction Accuracy Versus Sheet Impedance Level

In this section, to investigate the limits of the measurable impedance levels, we calculate the extraction errors of the proposed methods as functions of the sheet impedance. Since the error also depends on the frequency, the extraction errors are averaged in the studied band. The extraction errors of the real and imaginary parts of the impedance are denoted by $\mathcal{E}_{re}$ and $\mathcal{E}_{im}$, respectively, which are defined as follows:

$$\mathcal{E}_{re} = \frac{1}{N}\sum_{i=1}^{N}\frac{|\mathrm{Re}(\Delta Z_i)|}{|Z_{si}|} \qquad \mathcal{E}_{im} = \frac{1}{N}\sum_{i=1}^{N}\frac{|\mathrm{Im}(\Delta Z_i)|}{|Z_{si}|}. \quad (12)$$

Here, N is the number of the used frequency points. $\Delta Z_i = Z_{ei} - Z_{si}$ is the difference between the extracted and the exact values of the sheet impedance at the ith frequency point.

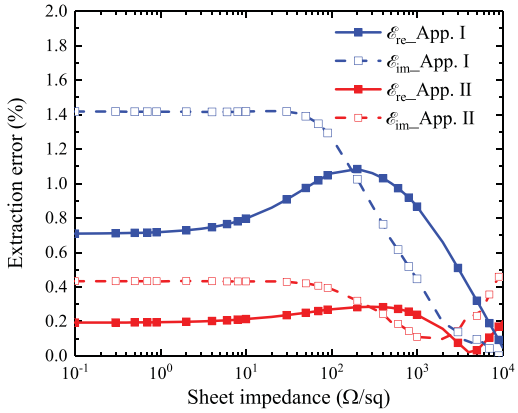

Fig. 6. Average errors of Approaches I and II within the frequency range (from 75 to 110 GHz) in terms of sheet resistivity (from 0.1 to 10^4 Ω/sq). Here, the gap thickness in simulations is assumed to be 125 μm.

Fig. 6 shows the extraction errors of the proposed approaches for resistive sheets (the reactive part of the impedance is set to zero). It can be observed in Fig. 6 that Approach II is better than Approach I in the estimation of both resistive and reactive parts of the sheet impedance. Notably, the extraction errors decrease rapidly when the resistivity is higher than 300 Ω/sq. This happens because as the sheet resistivity increases, the currents induced in the ink sheet become smaller, and the fields inside the measuring cell are less perturbed when the ink is introduced. As a result, the disagreement of the gap parameters between the two cases becomes smaller as the sheet impedance increases. From this analysis, we can see that the theoretical extraction errors are rather small (below 1.5%) in a wide resistivity range (from 0.1 to 10^4 Ω/sq). However, in practical measurements, the range of the measurable sheet impedances is smaller because of the uncertainty of measured scattering parameters, which will be discussed in the next section.

D. Extraction Accuracy Versus S-Parameters' Uncertainty

Vector network analyzer (VNA) measurement errors are classified into three main groups: systematic, random, and drift errors. Most of the systematic and drift errors can be removed by calibration and repeated measurements. However, random noise-type errors, which are unpredictable, lead to inevitable uncertainty of the measured scattering parameters.

In the retrieval of the ink properties using the methods proposed in this paper (Approaches I and II), two sets of error sources have to be considered: the naked substrate measurements ($|S_{11}|$, θ_{11}, $|S_{21}|$, and θ_{21}) and the conductive film measurements ($|S'_{22}|$, θ'_{22}, $|S'_{21}|$, and θ'_{21}). In particular, we focus our attention on the uncertainty analysis of Approach II. We use the differential uncertainty analysis, following the same procedure as in [21] and [22]. In this model, the dependent variable, Z_s, is differentiated with respect to each possible error sources (the magnitudes and phases of the S-parameters involved in the extraction method). Considering that each derivative can take positive and negative values, the final error is calculated as a sum of the squared values of all derivatives. Finally, the differential can be expressed as

$$\Delta Z_s = \sqrt{\sum_{\alpha}\left(\frac{\partial Z_s}{\partial|S_\alpha|}\Delta|S_\alpha|\right)^2 + \sum_{\alpha}\left(\frac{\partial Z_s}{\partial\theta_\alpha}\Delta\theta_\alpha\right)^2} \quad (13)$$

where index α corresponds to the four different S-parameters: S_{11}, S_{21}, S'_{21}, and S'_{22}. The partial differential can be calculated as

$$\frac{\partial Z_s}{\partial|S_\alpha|} = \frac{S_\alpha}{|S_\alpha|}\frac{K_\alpha}{F^2}, \quad \frac{\partial Z_s}{\partial\theta_\alpha} = jS_\alpha\frac{K_\alpha}{F^2}. \quad (14)$$

Here, $F = 1 - S'_{22} - S'_{21} - Z_0Y_{gp}(1 + S'_{22} + S'_{21})$, and K_α can be expressed as

$$\begin{aligned} K_{11} &= K_{21} = \frac{-2S'_{21}Z_0(1 + S'_{21} + S'_{22})}{(1 + S_{11} + S_{21})^2} \\ K'_{22} &= Z_0S'_{21}(1 + Z_0Y_{gp}) \\ K'_{21} &= K'_{22} + FZ_0. \end{aligned} \quad (15)$$

The uncertainties of S-parameters vary for different network analyzers and change with the magnitude of measured transmission or reflection coefficients. In practice, the uncertainty data ($\Delta|S_\alpha|$ and $\Delta\theta_\alpha$) are obtained from specifications of the network analyzer (in our case, Keysight E8361C, which is employed in our experiments).

In what follows, a comprehensive uncertainty analysis is applied to Approach II. Due to its importance in real applications, we will focus the analysis on the impedance determination of resistive sheets, assuming that the imaginary part is zero ($Z'_s = 0.1, \ldots, 1000\ \Omega/\text{sq}$ and $Z''_s = 0$). Two different studies will be done. First, we will study the individual effect of each parameter on the final extraction. Then, we will calculate the total effect when all the S-parameters are perturbed at the same time.

The effect of each individual S-parameter perturbation on the real and imaginary part errors is displayed in Fig. 7, assuming that the other parameters are unperturbed. When the sheet resistivity is smaller than 1000 Ω/sq, the extraction errors for both real and imaginary parts of the sheet impedance remain low (below 10%). In this range, the extraction error caused by S-parameters perturbations in the substrate characterization (S_{11} and S_{21}) is much smaller than that in the sample measurement. In particular, the perturbation errors in the substrate characterization can be neglected for sample resistances below 100 Ω/sq (the error is below 1%). It is also worth noting that the inaccuracy induced by S'_{21} perturbation

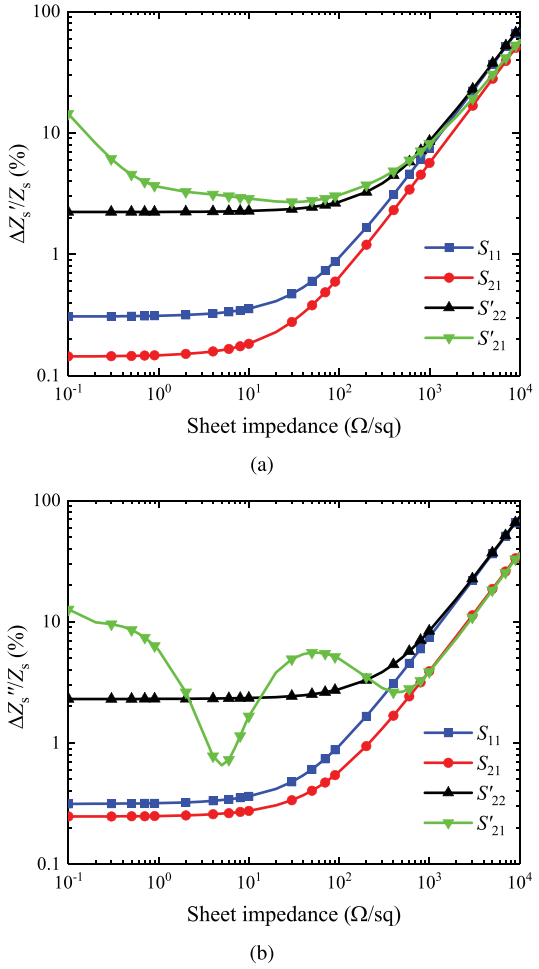

Fig. 7. Analysis of the individual uncertainty introduced by each S-parameter. (a) Real and (b) imaginary part errors of the extracted sheet impedance under the perturbations of S_{11}, S_{21}, S'_{22}, and S'_{21}. The studied sheet impedance varies from 0.1 to 10^4 Ω/sq. The substrate thickness is assumed to be 125 μm and the S-parameters are obtained at 95 GHz in simulation. The uncertainty of each S-parameter contains both amplitude and phase bounds.

increases when the sheet is highly reflective (below 1 Ω/sq). This is because both magnitude and phase perturbations of S'_{21} increase sharply when $|S'_{21}| \leq -50$ dB, according to the VNA specification. On the other hand, when the sheet resistivity is larger than 1000 Ω/sq, extraction errors also dramatically increase. It happens because the measured scattering parameters in film characterization become insensitive to the sheet impedance changes when its value is very large ($Z_s >$ 1000 Ω/sq). Therefore, a small uncertainty of S-parameters results in large extraction errors. Thus, although the extraction formulas become extremely accurate in this range of high impedances (see the previous section), inevitable measurement noise does not allow reliable extraction. For extremely high-impedance sheets (above about 1000 Ω/sq), resonant measurement methods should be used.

The total extraction errors considering the perturbations of all the S-parameters at the same time are calculated in Fig. 8. It is shown that the maximum measurement error of this method is around 10% for sheet resistance from 0.1 to 1000 Ω/sq.

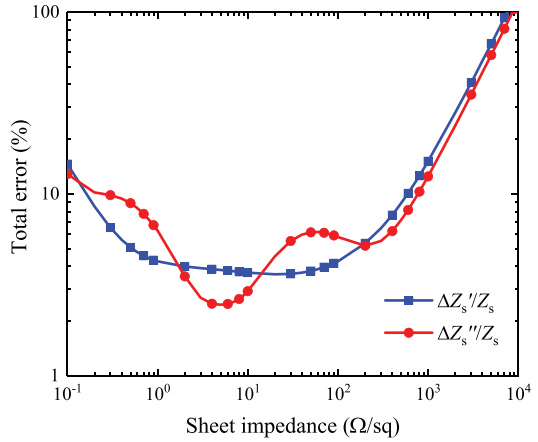

Fig. 8. Analysis of the total extraction uncertainty under the perturbation of all the S-parameters in terms of sheet resistivity (from 0.1 to 10^4 Ω/sq).

IV. Experimental Validation

This section presents the experimental results of sheet impedance extraction using the methods described above. Thin films used in our experiments are silver nanoparticles-based ink layers printed on a polyethylene naphthalate (PEN) substrate. For the system calibration, we choose the thru-reflect-line method, which is able to accurately correct both phase and magnitude errors introduced by sliding of the reference plane and the insertion loss of cables and connectors. Note that the metallic holders should be viewed as parts of the waveguide and included in the calibration process for removing their effects on the measurements. The experimental setup and the topology of metallic holder are shown in Fig. 9. The experiment steps comprise the following.

1) Adhere a bare PEN substrate to one of the metallic holders and ensure that the rectangular waveguide openings are completely covered by the substrate. The glue used for adhesion must be nonconductive with the thickness of several nanometers, so that it can be neglected in the ink impedance extraction.
2) Connect the two waveguide sections and measure both the magnitude and phase of the scattering parameters. Then, substitute the S-parameters in (2) and (3) and calculate the gap parameters Z_{g3} and Y_{gp}.
3) Cut a sample piece with printed ink and attach it to the holder. The size and thickness of the substrate should be the same as that used in Step 1, to create an identical gap structure. The size of ink sheet should be larger than the dimensions of waveguide cross section, to ensure its full coverage.
4) Connect the waveguides and measure the scattering parameters. Using (6) or (10), the ink impedance can be extracted.

A. Measurement of Gap Parameters

Fig. 10 shows the measured series and shunt impedances of the gap Π-circuit (Z_{g3} and $Z_{gp} = 1/Y_{gp}$). In order to verify the repeatability of Z_{g3} and Z_{gp} in separate measurements,

(a) (b)

Fig. 9. Photograph of (a) measurement setup and (b) metallic holder for WR10 waveguide. The sample is positioned between two such identical holders.

we conduct the experiment twice with the same substrate. Also, the value of Z_{gp} is simulated knowing the substrate thickness and permittivity (the substrate parameters used here are only for simulations, and they are not needed and not used in experimental extraction of the sheet impedance). Both simulation and experiment show that Z_{g3} is inductive and Z_{gp} is strongly capacitive. The disagreement between the numerical and two sets of experimental results of Z_{g3} in Fig. 10(a) is caused by differences of the gap structure in the simulation model and two measurements. In the experimental setup, it is difficult to keep the two holders perfectly parallel since the screws are fastened with somewhat different tightness. Also, holders can slightly bend when the screws are tightened. Strictly speaking, the thickness of the gap cannot be perfectly uniform everywhere inside the gap. Variations of the gap thickness contributed by these factors result in mismatch of Z_{g3} between the simulation and experiment and also between two measurements of the same sample.

Fig. 10(b) displays the measured and simulated shunt impedance of the gap Z_{gp}. Here, Z_{gp} can be viewed as a series connection of a resistor and a capacitor. The resistive part of Z_{gp} depends on the loss tangent of the substrate permittivity, and it is small for low-loss substrates. The capacitive part of Z_{gp} depends on the thickness of the substrate and also on the real part of the relative permittivity. The simulated and two separately measured results of Z_{gp} are almost the same. This fact confirms that Z_{gp} is repetitive and unchanged after successive assembling/disassembling of the setup. Unlike the extracted Z_{g3}, Z_{gp} is insensitive to setup flaws. This is because Z_{gp} is mostly determined by the field distribution in the cavity region (illustrated in Fig. 5), which is the least affected volume even if some misalignment or bending of the holders happens. The accurate estimation of Z_{gp} makes Approach II better than Approach I in sheet impedance extraction, which will be discussed later.

B. Measurement of Ink Impedance

After determining the gap parameters, the sheet impedance of the ink can be extracted by the two different approaches proposed in Section II. Fig. 11(a) shows the retrieved sheet impedance of a sample with Z_s= 4.5 Ω/sq (sample S1) measured under dc condition. The ink layer is printed using RO technology and cured for 60 min under 180 °C. The substrate of the ink sheet is a single-layer PEN that has

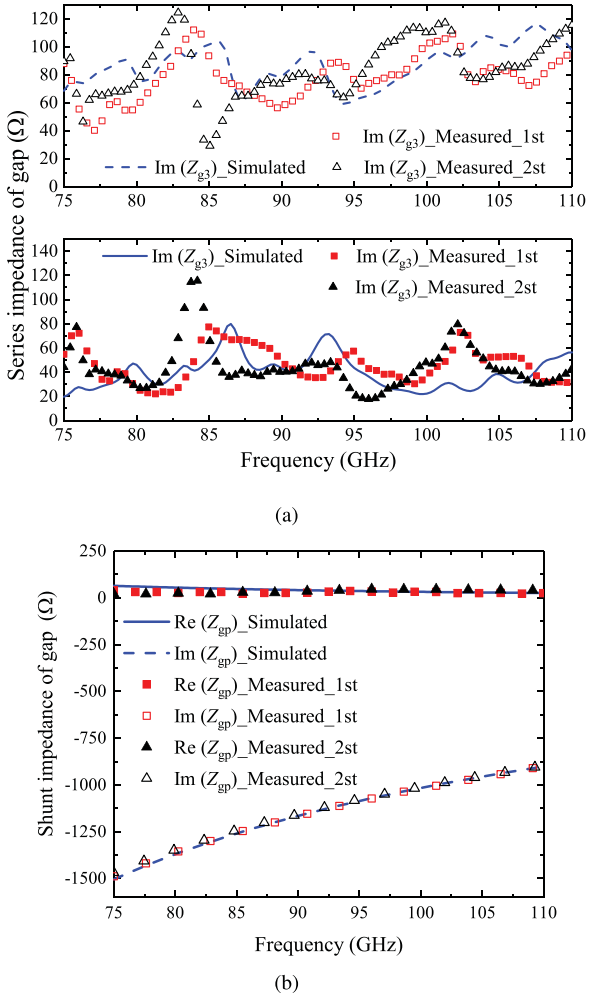

Fig. 10. Simulated and measured values of the gap parameters. (a) Z_{g3}. (b) Z_{gp} ($Z_{gp} = 1/Y_{gp}$). Two independent measurements are conducted here with the same substrate. The substrate inside gap is PEN with the thickness $d = 125\ \mu$m and the permittivity $\epsilon_r = 3.2(1-j0.045)$. The substrate size is 10.5 mm × 8 mm.

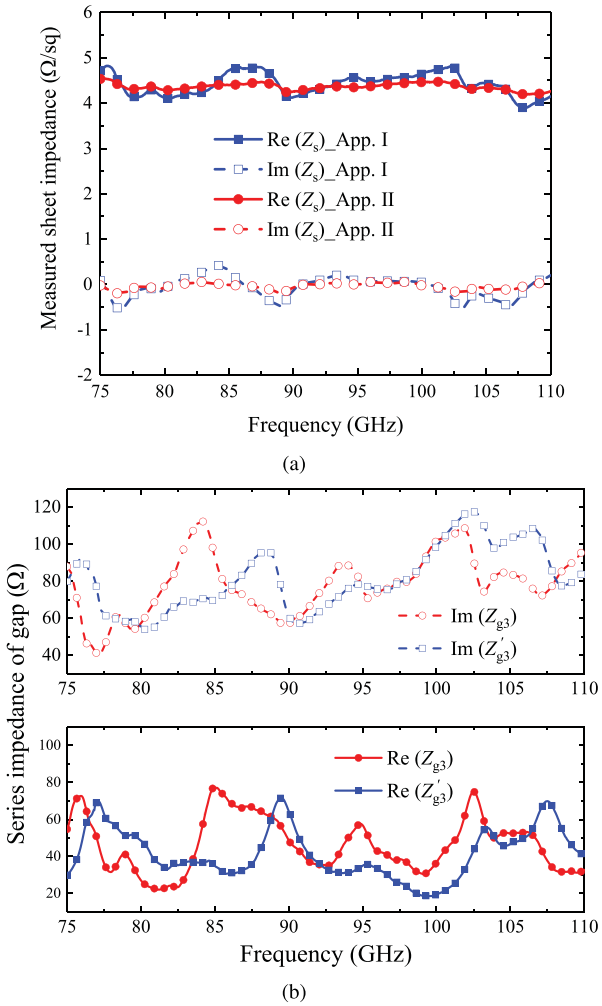

Fig. 11. (a) Extracted sheet impedance of sample S1 using Approaches I and II. Here, Z_s is measured to be 4.5 Ω/sq via dc method. (b) Extracted Z'_{g3} and Z_{g3} for sample S1.

the same physical parameters as the substrate analyzed in Section IV-A.

As expected, it is evident in Fig. 11(a) that extraction using Approach II is more accurate than Approach I, which suffers from perturbations in both real and imaginary parts of the extracted value. The fluctuations of the extracted impedance using Approach I are a consequence of the assumption that $Z'_{g3} = Z_{g3}$. Note that Z'_{g3} can also be solved from (8) and (9), and we plot the extracted Z'_{g3} and Z_{g3} in Fig. 11(b). The two curves do not overlap. The difference of Z'_{g3} and Z_{g3} in the considered frequency range is reflected in the perturbations of the extracted ink impedance. It is interesting to note that the difference in the real part of Z'_{g3} and Z_{g3} results in the perturbations of the sheet resistance, while the imaginary part affects the sheet reactance. The differences of Z'_{g3} and Z_{g3} are partly due to the changes of the field distribution in the dielectric layer when a conductive ink sheet is attached to it. In addition, it is also influenced by the unperceived changes of the experimental setup such as unparallel placement and bending of the holders.

In order to illustrate the extraction capability of Approach II in the case of thick substrates, three additional PEN layers are added to sample S1 creating a thick substrate with $d = 500\ \mu$m (about $0.28\lambda_d$). The measured results using Approach II and the method proposed in [10] are compared in Fig. 12(a). Obviously, for a thick substrate, the extraction method in [10] is totally invalid, and the extracted curves deviate from the expected value with severe oscillations. The uneven results are directly reflected in the multiple resonances in the transmission spectrum [see Fig. 12(b)], which are triggered by the reflections of the TEM wave traveling inside the gap. However, Approach II still demonstrates its accuracy and stability within the whole frequency band. For Approach II, the poles in the transmission coefficient are compensated for by introducing S'_{22} to (10), resulting in a smooth impedance curve.

To demonstrate the validity of Approach II in a wide range of sheet impedances, we have measured three samples with ink sheets cured at different thermal conditions after printing. It is known that the resistivity of printed ink sheets decreases with

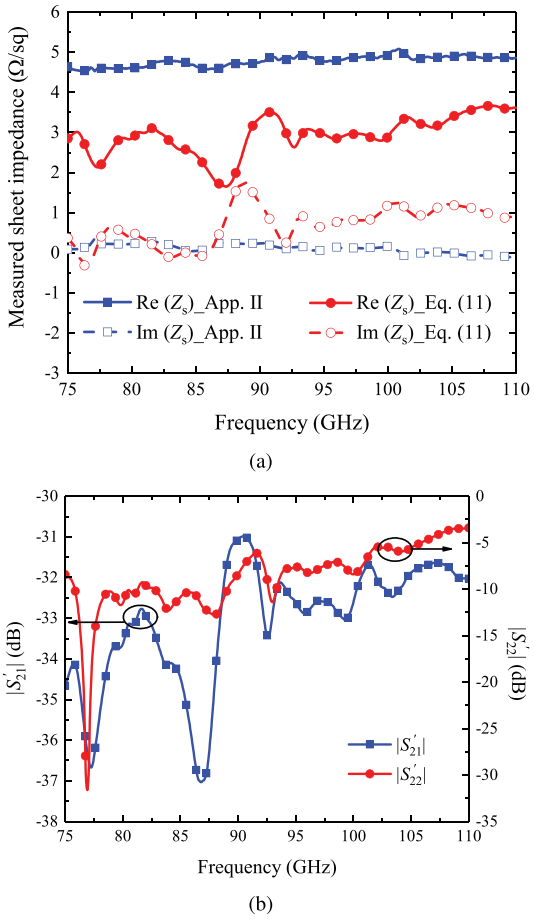

Fig. 12. (a) Measured results for sample S1 with four-layer substrates using Approach II and the method in [10]. The ink impedance is $Z_S = 4.5\ \Omega$/sq predicted under dc condition. (b) Measured scattering parameters of sample S1 with four PEN layers.

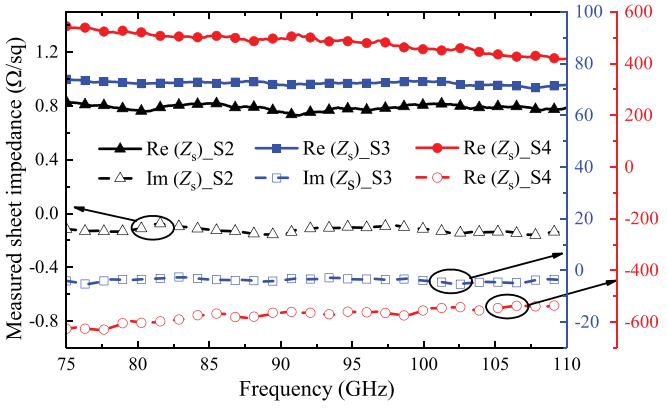

Fig. 13. Measured sheet impedance of samples S2–S4 that have been sintered for 60, 25, and 20 min in a 180 °C oven, respectively. The values have been extracted using Approach II. The left, right-inside, and right-outside scale refer to samples S2–S4, respectively.

increasing the sintering temperature and time. The measured samples (samples S2–S4) are sintered for different times in a 180 °C heating environment. As is seen from Fig. 13, the sheet impedance of sample S2, treated for 60 min, is rather low, about $0.8 - 0.1j\ \Omega$/sq. When the sintering time decreases to 25 min, the sheet impedance increases to around $71 - j3\ \Omega$/sq (sample S3). For samples S2 and S3, the resistive parts of the sheet impedance are much larger than the reactive parts, and the extracted curves are almost flat in the frequency of interest. The measured resistivity of samples S2 and S3 under dc conditions is 0.8 and 71.5 Ω/sq, respectively. When the sintering time reduces to 20 min, both the resistive and capacitive parts increase dramatically and exhibit a frequency-dependent behavior.

V. Conclusion

We have proposed and developed a method to accurately measure complex sheet impedances of electrically thin conductive layers supported by dielectric substrates using a simple rectangular waveguide setup. Using an equivalent circuit of the gap formed by two waveguide flanges and the dielectric substrate, we can successfully remove the effect of the waveguide gap without a separate characterization of the thickness and permittivity of the substrate. Based on this principle, two retrieval approaches using different assumptions for the gap parameters have been proposed and compared. The influence of the uncertainties in the measured S-parameters on the extraction accuracy has also been examined. The experimental results of ink sheet impedance measurements with thick and thin substrates successfully demonstrated the capability of the method to extract the surface impedance. Since the method is applicable to a wide range of complex sheet impedances, it is important to mention that the introduced method is not limited to measurements of conductive inks, but it can be used for studies of various electrically thin sheets at microwave and millimeter-wave frequencies, for example, silver nanowire composites or graphene or other carbon-based layers.

Acknowledgment

The authors would like to thank S. Khanal, I. Nefedova, and J. Ala-Laurinaho for their help in measurements, and V. Asadchy for technical discussions. The authors would also like to thank A. Sneck, A. Alastalo, and T. Mäkelä, VTT Technical Research Center of Finland, for providing ink samples and also for making dc measurements of the samples.

References

[1] N. Pompeo, R. Marcon, and E. Silva, "Dielectric resonators for the measurement of superconductor thin films surface impedance in magnetic fields at high microwave frequencies," *J. Supercond. Novel Magn.*, vol. 20, no. 1, pp. 71–82, Jan. 2007.

[2] J. Krupka and J. Mazierska, "Contactless measurements of resistivity of semiconductor wafers employing single-post and split-post dielectric-resonator techniques," *IEEE Trans. Instrum. Meas.*, vol. 56, no. 5, pp. 1839–1844, Oct. 2007.

[3] J. Krupka, "Measurement of the complex permittivity of metal nanoislands and the surface resistance of thin conducting films at microwave frequencies," *Meas. Sci. Technol.*, vol. 19, no. 6, Apr. 2008, Art. no. 065701.

[4] J. Krupka and W. Strupinski, "Measurements of the sheet resistance and conductivity of thin epitaxial graphene and SiC films," *Appl. Phys. Lett.*, vol. 96, no. 8, Feb. 2010, Art. no. 082101.

[5] A. I. Gubin *et al.*, "Whispering-gallery-mode resonator technique with microfluidic channel for permittivity measurement of liquids," *IEEE Trans. Microw. Theory Techn.*, vol. 63, no. 6, pp. 2003–2009, Jun. 2015.

[6] H. Skulason *et al.*, "110 GHz measurement of large-area graphene integrated in low-loss microwave structures," *Appl. Phys. Lett.*, vol. 99, no. 15, Oct. 2011, Art. no. 153504.

[7] M. W. Hyde, M. J. Havrilla, and P. E. Crittenden, "A novel method for determining the R-card sheet impedance using the transmission coefficient measured in free-space or waveguide systems," *IEEE Trans. Instrum. Meas.*, vol. 58, no. 7, pp. 2228–2233, Jul. 2009.
[8] M. Liang *et al.*, "Terahertz characterization of single-walled carbon nanotube and graphene on-substrate thin films," *IEEE Trans. Microw. Theory Techn.*, vol. 59, no. 10, pp. 2719–2725, Oct. 2011.
[9] R. J. Collier and D. C. Hasko, "Measurement of the sheet resistance of resistive films on thin substrates from 120 to 175 GHz using dielectric waveguides," *J. Appl. Phys.*, vol. 91, no. 4, pp. 2547–2549, Feb. 2002.
[10] F. Costa, "Surface impedance measurement of resistive coatings at microwave frequencies," *IEEE Trans. Instrum. Meas.*, vol. 62, no. 2, pp. 432–437, Feb. 2013.
[11] J. S. Gómez-Díaz, J. Perruisseau-Carrier, P. Sharma, and A. Ionescu, "Non-contact characterization of graphene surface impedance at micro and millimeter waves," *J. Appl. Phys.*, vol. 111, no. 11, Jun. 2012, Art. no. 114908.
[12] R. Parashkov, E. Becker, T. Riedl, H. H. Johannes, and W. Kowalsky, "Large area electronics using printing methods," *Proc. IEEE*, vol. 93, no. 7, pp. 1321–1329, Jul. 2005.
[13] J. Perelaer *et al.*, "Printed electronics: The challenges involved in printing devices, interconnects, and contacts based on inorganic materials," *J. Mater. Chem.*, vol. 20, no. 39, pp. 8446–8453, Jun. 2010.
[14] A. V. Räisänen *et al.*, "Suitability of roll-to-roll reverse offset printing for mass production of millimeter-wave antennas: Progress report," in *Proc. Antennas Propag. Conf. (LAPC)*, Loughborough, U.K., Nov. 2016, pp. 300–304.
[15] P. F. Moonen, I. Yakimets, and J. Huskens, "Fabrication of transistors on flexible substrates: From mass-printing to high-resolution alternative lithography strategies," *Adv. Mater.*, vol. 24, no. 41, pp. 5526–5541, Nov. 2012.
[16] S. Khan, L. Lorenzelli, and R. S. Dahiya, "Technologies for printing sensors and electronics over large flexible substrates: A review," *IEEE Sensors J.*, vol. 15, no. 6, pp. 3164–3185, Jun. 2015.
[17] F. C. Krebs, "Fabrication and processing of polymer solar cells: A review of printing and coating techniques," *Solar Energy Mater. Solar Cells*, vol. 93, no. 4, pp. 394–412, Apr. 2009.
[18] W. Clemens, W. Fix, J. Ficker, A. Knobloch, and A. Ullmann, "From polymer transistors toward printed electronics," *J. Mater. Res.*, vol. 19, no. 7, pp. 1963–1973, Jul. 2004.
[19] D. Kim and J. Moon, "Highly conductive ink jet printed films of nanosilver particles for printable electronics," *Electrochem. Solid-State Lett.*, vol. 8, no. 11, pp. J30–J33, Nov. 2005.
[20] D. M. Pozar, *Microwave Engineering*. New York, NY, USA: Wiley, 2009.
[21] J. M. Catala-Civera, A. J. Canos, F. L. Penaranda-Foix, and E. de los R. Davo, "Accurate determination of the complex permittivity of materials with transmission reflection measurements in partially filled rectangular waveguides," *IEEE Trans. Microw. Theory Techn.*, vol. 51, no. 1, pp. 16–24, Jan. 2003.
[22] A. H. Boughriet, C. Legrand, and A. Chapoton, "Noniterative stable transmission/reflection method for low-loss material complex permittivity determination," *IEEE Trans. Microw. Theory Techn.*, vol. 45, no. 1, pp. 52–57, Jan. 1997.

Xu-Chen Wang received the B.Sc. degree in optical information science and technology from Northwestern Polytechnical University, Xi'an, China, in 2011, the master's degree from the Department of Optical Engineering, Zhejiang University, Hangzhou, China, in 2014, and is currently pursuing the D.Sc. degree under supervision of Prof. S. Tretyakov at the Department of Electronics and Nanoengineering, School of Electrical Engineering, Aalto University, Aalto, Finland.

He was a Radio Frequency Engineer with Huawei and TP-Link from 2014 to 2016. His current research interests include flexible metasurfaces, absorbers, and antennas at terahertz frequencies.

Ana Díaz-Rubio was born in Landete, Spain. She received the bachelor's degree in telecommunication engineering, M.Sc. degree, and Ph.D. degree from the Polytechnic University of Valencia, Valencia, Spain, in 2010, 2011, and 2015, respectively.

She is currently a Post-Doctoral Researcher under the supervision of Prof. S. Tretyakov with the Department of Electronics and Nanoengineering, School of Electrical Engineering, Aalto University, Aalto, Finland. Her current research interests include artificial thin surfaces for controlling the wave propagation.

Dr. Díaz-Rubio was a recipient of the FPI-MEC Fellowship from the Science and Innovation Ministry of Spain of the Polytechnic University of Valencia in 2011, where she was supervised by Prof. J. S.-Dehesa.

Sergei A. Tretyakov (M'92–SM'98–F'08) received the Dipl.Eng. degree in engineering physics (with a specialization in radiophysics), Candidate of Sciences (Ph.D.) degree in radiophysics, and D.Sc. degree in radiophysics from St. Petersburg State Technical University, St. Petersburg, Russia, in 1980, 1987, and 1995, respectively.

From 1980 to 2000, he was with the Radiophysics Department, St. Petersburg State Technical University. He was a Visiting Scientist with CEA-CESTA (French Atomic Energy Commission Research Center), also affiliated with the Laboratory of Wave-Material Interactions, University of Bordeaux, in 1994, and as a Visiting Professor with the Abbe Center of Photonics, Friedrich Schiller University Jena, Jena, Germany, and with the Department of Photonics Engineering, Technical University of Denmark, Kongens Lyngby, Denmark, in 2013. He is currently a Professor of radio engineering with the Department of Electronics and Nanoengineering, Aalto University, Aalto, Finland. His current research interests include electromagnetic field theory, complex media electromagnetics, and microwave engineering.

Prof. Tretyakov served as the President of the European Virtual Institute for Artificial Electromagnetic Materials and Metamaterials (Metamorphose VI) during 2007–2013 and as the Chairman of the St. Petersburg IEEE ED/MTT/AP Chapter from 1995 to 1998. He was the General Chair of the conference series Congress on Advanced Electromagnetic Materials in Microwaves and Optics (Metamaterials) during 2007–2014.